Measurement of wave crest length and groupiness from spaceborne Synthetic Aperture Radar

F. Monaldo

The Johns Hopkins University Applied Physics Laboratory, Laurel, MD, USA

Abstract. Most measurements of ocean surface wave variations are made in the temporal domain, *i.e* wave height or slope as a function of time. By contrast, a synthetic aperture radar (SAR) is capable of measuring waves in the two-dimensional spatial domain at essentially a single instant. As a consequence, SAR imagery affords us a unique opportunity to examine some of the non-linear features of ocean surface waves. In this paper, we use spaceborne SAR imagery from the Shuttle Imaging Radar-B (SIR-B) mission to estimate wave crest length and groupiness. These features may contribute to the likelihood of encountering an especially devastating large wave. After providing a specific procedure for objectively computing these quantities, we find that the crest lengths are longer and groupiness more prevalent that one would expect based on linear wave theory.

Introduction

The examination of the question of "rogue" or unexpectedly high ocean waves pushes us to the extremes of both theory and measurement. On the one hand, useful approximations of linear wave theory or weakly nonlinear interactions may break down under the extreme conditions associated with rogue waves. On the other hand, wave measurement instrumentation, accurate for conventional waves, may degrade under extreme conditions. Moreover, the measurement of extreme waves, even when not encumbered with instrument errors, occurs sufficiently infrequently that it is difficult to draw meaningful conclusions. One embarks on the study of rogue waves cautioned by the observation attributed to Nobel Prize-winning English chemist Sir Cyril Hinshelwood that the world is "... divided into hydraulic engineers who observed things that could not be explained and mathematicians who explained things that could not be observed." It is likely, therefore, that, in the short term, we will only be able to address the questions surrounding rogue waves indirectly and by inference.

If the ocean surface behaved linearly, if the waves associated with individual frequency components summed up independently, the question of predicting the frequency of occurrence of rogue waves would be straightforward. One could take empirical or model ocean wave spectra, associate uniformly distributed random phase elements with each spectral element and create simulated wave surfaces. The probability of encountering especially large waves, by whatever convenient criteria one might choose, could be determined from the statistics of such simulated surfaces.

Waves, however, behave in accordance with their own physics, and are not constrained by what is convenient for us to compute. Waves interact nonlinearly and a number of investigators have suggested that these may contribute to an increased occurrence of rough waves [*Forristall*, 2000].

Here we consider two properties that are a function of nonlinear wave interaction and that may play a role in the appearance of rogue waves: "long-crestedness" and "groupiness" [*Kriebel and Dawson*, 1991]. A monochromatic have would have an infinitely long crest. Crest lengths are controlled by the broadness of the wave spectrum and the interaction between waves. Groupiness is a measure of the common observation that especially large waves can group together. Groupiness is also dependent upon the degree nonlinear wave interaction.

In this paper, we describe how synthetic-aperture radar (SAR) imagery can be used make spatial measurements of waves, explain quantitative measures of long-crestedness and groupiness, and demonstrate that by such measures the observed long-crestedness and groupiness are greater than would be expected on the basis of linear wave theory. This work is an outgrowth of work performed by *Monaldo* [2000] to assess the effect of ocean surface waves on large mobile offshore platforms.

SAR wave imagery

To understand SAR wave imagery, it is perhaps best to begin by consideration of a real-aperture side-looking radar on a spaceborne or airborne platform. As the platform flies in a straight line, a side-looking radar will image a swath on the Earth's surface. Range resolution, or resolution perpen-

dicular to the flight path, is obtained from fine-scale timing. The distance from the platform to a point in the image swath is determined by the return-trip travel time. For a real aperture radar, azimuth, or along-the-flight-path direction, resolution is limited by the beam-width of the radar.

The angular beamwidth of a radar is approximately equal to the ratio of the radar wavelength to aperture size, λ/D. Spaceborne SARs have operated at L-band (20 cm wavelength) and C-band (5 cm wavelength). Even at C-band with at 10 m long antenna, the angular field of view would be 0.005 radians. At a range of about 1000 km from the surface, typical for spaceborne SARs, this angular resolution would correspond to 5000 m azimuth resolution on the surface, much too coarse to image waves and much larger than the typical 25-m range resolutions possible. However, by recording the received signal as the platform flies along, it is possible to "synthesize" the signal that might have been received by a kilometers-long antenna. The result is the ability of a SAR to create high-resolution radar cross-section images of the ocean surface.

At moderate incident angles, 20° to 60°, the normalized radar cross section of the ocean surface is related to the surface roughness on the scale of the radar wavelength projected on the surface, through a "Bragg resonance." These short waves are often referred to a "Bragg waves" [*Wright*, 1960, 1968]. The rougher the surface the higher the cross section. As a consequence, radar backscatter has been used to estimate wind speed. However, anything that modulates these short waves or their aspect with respect to the radar will be imaged.

Ocean waves have long been known to be visible in SAR images. Indeed, the original purpose of the SAR on the Seasat satellite in 1978 was to image ocean waves. For long ($>$ 50 m) waves traveling in the range direction, the local incident angle at the surface is modulated and so is radar cross section. In addition, Bragg waves are modulated by a hydrodynamic interaction with the longer underlying long waves. To first order, this radar cross-section modulation in the range direction is proportional to long wave slope.

The imaging of azimuth-traveling waves is more intimately tied to the way a SAR achieves high azimuth resolution. Consider for example a single bright scatterer within a SAR image swath. As the SAR platform passes past the point, the relative velocity or Doppler frequency changes, reaching zero when the along track position of the SAR and the scatterer coincide. It is at this azimuth position that the scatterer is located in the SAR image. If the scatterer is moving towards or away from the radar, then the position of zero Doppler shift will be different and the scatterer will be placed at a different azimuth position in the image. The azimuth position shift is equal to Rv_r/V where R is the range between the satellite and the surface, V is the platform velocity and v_r, the velocity component in the radar line-of-sight direction [*Harger*, 1970].

This repositioning of reflected energy can make azimuth-traveling waves visible in SAR imagery. The orbital velocity of the ocean surface waves imposes a velocity on the Bragg waves and causes their apparent positions in the SAR image to be displaced. The periodic variation in velocity concentrates and dissipates the the density of surface scatterers at the same spatial frequency as the long ocean waves, rendering azimuth-traveling waves visible [*Alpers and Ruffenach*, 1979; *Swift and Wilson*, 1979].

To first order, the change in apparent radar cross section with for azimuth-traveling waves is also proportional to long wave slope. However, when the wave heights get too large, wave orbital velocities also grow large, and the scatterers can be shifted more than one long ocean wavelength in azimuth. This effectively degrades azimuth resolution. *Beal et al.* [1983] empirically showed that the minimum detectable azimuth wavelength by a SAR, $\lambda_{\min}$ is given by

$$\lambda_{\min} = 1[\mathrm{m}^{1/2}/\mathrm{s}]\frac{R}{V}H_s^{1/2} \qquad (1)$$

where H_s is ocean significant wave height.

This latter limitation is a crucial factor in SAR wave images. For polar-orbiting free-flying SAR satellites, R/V is about 120 s. For a $H_s = 4$ m, the minimum detectable azimuth wavelength is 240 m, with resolution further degrading in higher sea states. Fortunately, in 1984 and twice in 1994, NASA flew SARs on space shuttles in low 220-km orbits, as part of the Shuttle Imaging Radar (SIR-B and SIR-C) missions. At this low altitude, R/V was approximately 35 s. Now in a 4-m sea state, the minimum detectable wavelength decreases from 240 m to 70 m, drastically increasing the SAR's ability to measure waves in high sea states. A comprehensive discussion of SAR wave imagery can be found in *Lehner and Ocampo-Torres* [2003].

In this paper, we consider SIR-B imagery in the vicinity of Hurricane Josephine from October 12, 1984. We use these data to make estimates of ocean wave crest lengths and groupiness.

Estimation of crest lengths

Procedure

Typically, crest lengths are a function of the shape of the wave spectrum. Narrow wave spectra produce long-crested waves. Broad spectra result in shorter wave crests. In the obvious narrow-spectrum limit of a single spectral component — a sine wave — the crest lengths are infinite. The phases of the individual wave spectral elements also contribute to crest length. Here we explain a procedure for estimating crest length that produces repeatable results that are consistent with human eye estimates of crest length. Figure 1 illustrates the estimation of crest lengths. The left side of

Figure 1 is a gray-scale representation of a sample 3.2×3.2 km SAR image in the vicinity of Hurricane Josephine on October 12, 1984. Waves are clearly visible.

The estimation of crest length statistics from wave imagery relies on two basic steps: the filtering of imagery so that crests are conspicuously identified as separate "blobs" and the estimation of crest length statistics from these blobs. Though the procedures are applied here to SAR imagery, they can be applied in general to any spatial image of waves.

We begin by Fourier transforming the SAR intensity image (proportional to normalized radar cross section). Let $I(x,y)$ represent SAR image intensity a function of range, x, and azimuth, y, position. $F(k_x,k_y)$ is the Fourier transform of I where k_x and k_y are range and azimuth wavenumber, respectively.

We then construct a high-pass filter, $H_1(k_x,k_y)$, such that

$$H_1(k_x,k_y) = \begin{cases} 1 & \text{if } k > k_{\min} \\ 0 & \text{otherwise} \end{cases} \quad (2)$$

where k is wavenumber magnitude and $k_{\min}$ represents the smallest wavenumber of interest. Essentially, we eliminate low spatial frequency variations of SAR image intensity. Typically, we set $k_{\min} = 2\pi/1600$ m. Image variations at wavelengths longer than 1600 m are thus removed.

We remove some of the remaining image speckle noise by thresholding the image spectrum, $S(k_x,k_y)$, which is given by

$$S(k_x,k_y) = F(k_x,k_y)F^*(k_x,k_y)\ . \quad (3)$$

The threshold level, T_s is given by $T_s = \mu_s + A\sigma_s$ where A is an adjustable parameter, and μ_s and σ_s are the mean and standard deviation of the spectral values, respectively. Setting $A = 3$ has proven successful for eliminating speckle noise. We now define a second spectral filter as.

$$H_2(k_x,k_y) = \begin{cases} 1 & S(k_x,k_y) > T_s \\ 0 & \text{otherwise}\ . \end{cases} \quad (4)$$

We apply these filters to the original Fourier transform and compute a new Fourier transform, $F'(k_x,k_y)$ given by

$$F'(k_x,k_y) = H_1(k_x,k_y)H_2(k_x,k_y)F(k_x,k_y)\ . \quad (5)$$

The inverse Fourier transform of $F'(k_x,k_y)$ produces an image from which low-frequency variations are removed and image noise alleviated. Of course, this resulting image shows continuous intensity variations. To define crest areas, we threshold the image using a level T_I, defined by $T_I = \mu_I + B\sigma_I$ where B is an adjustable parameter, that we have set to 1. Images values above the threshold are considered crests.

On the right side of Figure 1, every pixel either is or is not identified as part of a crest. Each spatially contiguous set of pixels identifies a crest area, which we call a "blob." At this point, we fit each blob to an ellipse and compute the semi-major and semi-minor axes, the eccentricity, and the orientation of the ellipses. Ellipses that cover an area greater than 150 m^2 and that are oriented within 15° of the dominant wave direction are retained.

Crest length results

We applied this procedure to estimate the long-crestedness of waves in the vicinity of Hurricane Josephine. However, the real question is how these results compare with what we might have expected purely on the basis of the spectral width. To simulate this, we begin with a spectrum computed from an observed image. We assume that this spectrum is but a single realization of the ensemble mean spectrum which represents the surface.

In this single realization, each spectral element is a random variable having a χ^2-distribution with two degrees of freedom. The mean of this distribution is the ensemble mean spectral value. We approximate this ensemble mean spectrum by smoothing the observed spectrum with a 20×20-pixel Gaussian filter. We can then simulate an ensemble of spectra whose mean is consistent with the observed spectrum. For each spectrum in the ensemble, every spectral element has an independent phase.

Figure 2 is a plot of the number of crests per unit area having a crest length longer than the abscissa. The solid line was computed for a SIR-B SAR image in the vicinity of Hurricane Josephine. The light gray lines represent the result of simulations. Whether because long wave dispersion has caused the phasing of the wave components to be correlated or because of nonlinear wave-wave interaction, the SAR wave imagery considered here show crest lengths substantially longer than would have been expected on the basis of the shape of the wave spectrum alone. Although we have not applied a formal statistical significance test, it is clear from Figure 2 that the observed long-crestedness is not from the same population as the simulated estimates.

Wave groupiness

If waves at different wavelengths are independent of one another, one consequence is a Gaussian distribution of wave heights and wave slopes. Examining wave buoy wave records, *Phillips et al.* [1993] compared deviations of mean wave profiles from Gaussian statistics. If wave heights have a Gaussian distribution, it is possible to estimate the likelihood of encountering an especially large wave and the likelihood of a sequence of large waves. *Phillips et al.* [1993] found reasonable agreement between the buoy records and their expectations for a Gaussian sea.

Phillips et al. [1993] related the mean height profile of the surface to the temporal autocorrelation function of the wave field. Here, we are not limited to a temporal wave field

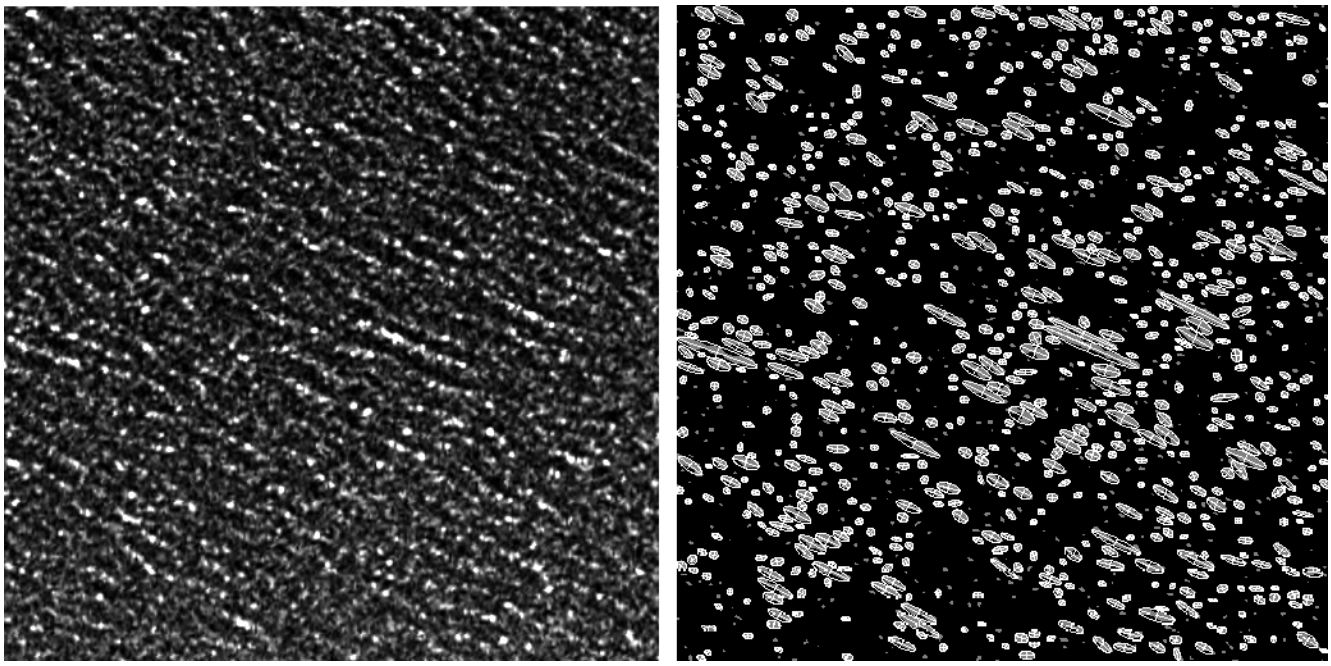

Figure 1. Sample image acquired from SIR-B of waves in the vicinity of Hurricane Josephine. This image covers 256×256 pixels or 3.2×3.2 km in area. The left side is the original SAR image intensity. The right side shows the wave crests in light gray that have been fitted to ellipses outlined in white.

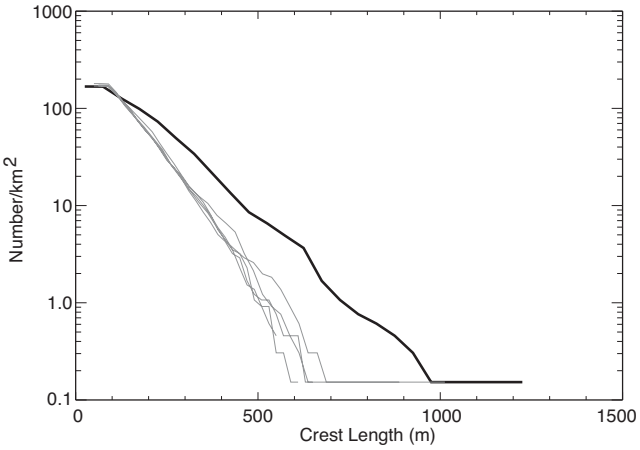

Figure 2. The number of crests per unit area having a crest length longer than the abscissa. The thick line represents the estimate from the data, the lines represent the predictions of simulations. Data were acquired in the vicinity of Hurricane Josephine.

from buoy data, but are afforded the luxury of a full two-dimensional spatial wave field. In keeping with the developments of *Phillips et al.* [1993], we decided to use the spatial autocorrelation of the wave field, as measured by a SAR, to determine if large waves are likely to group together.

Nonetheless, the use of autocorrelation techniques, assumes that the ocean surface is spatially stationary. Questions of ocean wave spatial and temporal stationarity and wave groupiness were considered by *Donelan et al.* [1996] and *Molle-Christensen and Ramamonjiarisoaas* [1978].

To first order and especially for SAR geometries having low R/V ratios, image intensity is proportional to wave slope. We begin by assuming here that this is true. Later in this paper, we will return to this question and demonstrate that this assumption does not lead us to any false conclusions.

Let $I(x,y)$ be a two-dimensional image intensity field that is a function of coordinates x and y. In general, the normalized autocorrelation function is represented by

$$R(x',y') = \frac{\int_0^X \int_0^Y I(x,y)I(x+x',y+y')dxdy}{XY\sigma_I^2} \qquad (6)$$

in the limit of X and Y going to infinity. The quantity σ_I^2 is the variance of $I(x,y)$ and X and Y are the lengths of the two-dimensional field in the x and y directions, respectively. This function describes how correlated different parts of the image are when separated by x' and y'.

As $x' = y' = 0$, $R(x',y')$ goes to 1. A point is perfectly correlated with itself. For purposes of computational efficiency, autocorrelation functions were computed from the spectrum of the image. If we allow $I(x,y)$ to represent an image, $F(k_x,k_y)$ its Fourier transform, and $S(k_x,k_y) = F(k_x,k_y)F^*(k_x,k_y)$ its spectrum, then the autocorrelation function can be written as

$$R(x',y') = \mathrm{F}^{-1}\{S(k_x,k_y)\}\ , \tag{7}$$

the inverse Fourier transform of the spectrum [*Bendat and Piersol*, 1993].

We now compute the spatial autocorrelation function of the SIR-B SAR image shown in Figure 1. We first remove the low-frequency energy in the spectrum for wavelengths longer than 1600 m. We then compute the two-dimensional autocorrelation function. The result is shown in Figure 3. Zero spatial lag is at the center of Figure 3. Note that the autocorrelation function shows oscillatory behavior near zero lag. A wave crest at any particular position is correlated with other wave crests, one, two, or more wavelengths away. The correlation decreases for larger lags.

To make the groupiness measured by the spatial autocorrelation more apparent, we rotate the autocorrelation function in Figure 3 so that the wave propagation direction is vertical. The autocorrelation function is then averaged along the horizontal direction. Figure 4 is the result. The oscillations in this curve every few hundred meters are clearly visible. In addition, there is an envelope modulating these oscillations. This envelope has a spatial wavelength of approximately 2500 m. This suggests the ocean waves in this scene group together in groups of 2500 m in length. This envelope modulation does not appear when the autocorrelation function is projected in other directions.

Before we can draw conclusions about ocean surfaces, we need to understand whether the observed behavior of the autocorrelation function is a consequence of the waves on the surface or an artifact of either the image processing steps applied to SAR imagery or to non-linearities in the SAR wave imaging process.

To test the dependence of these results on high-pass filtering, we applied high-pass filters with various low-wavenumber cutoffs. Figure 5 is a plot of the collapsed autocorrelation function for different low-wavenumber cutoffs, ranging from 4000 to 100 m

Note that the modulating envelope remains the same independent of the high-pass cutoff wavelength, until we employ a cutoff of $\lambda_c = 100$ m. Thus, these measurements of groupiness are robust in the face of different levels of smoothing.

It is possible that the cause of the observed groupiness is phase correlations between different waves components adding up so as to make waves bunch into groups. If each component in the wave spectrum has a phase that was uncor-

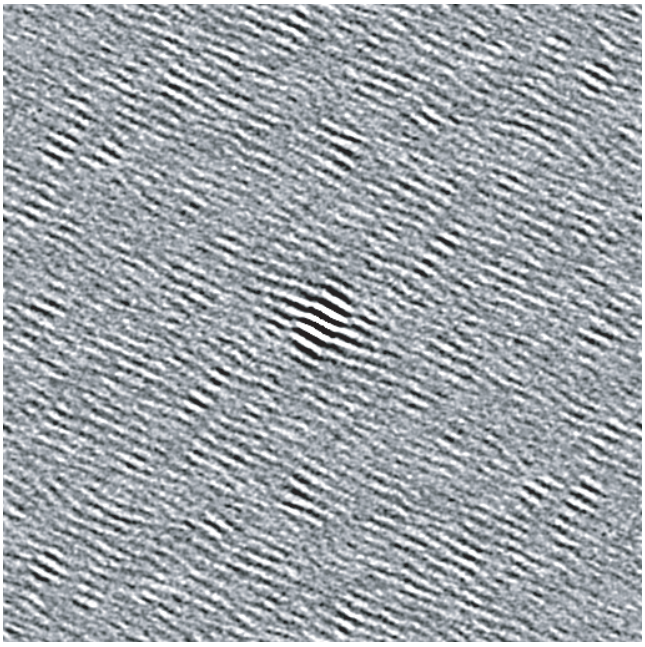

Figure 3. Two-dimensional autocorrelation of a SIR-B SAR image in the vicinity of Hurricane Josephine. The center of the image represents zero spatial lag.

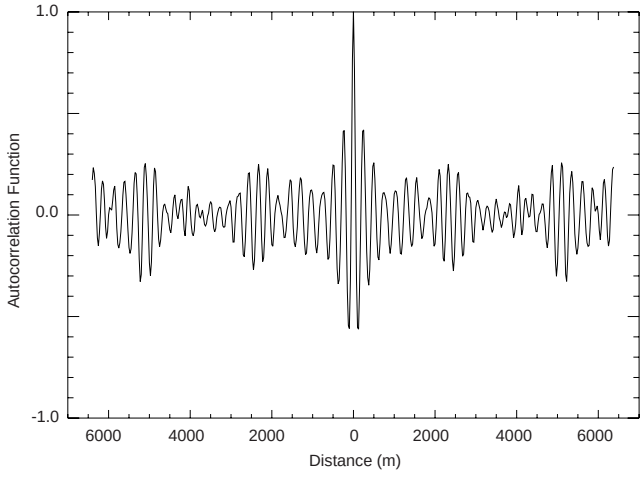

Figure 4. One-dimensional projection of the autocorrelation function versus lag distance computed from the two-dimensional autocorrelation function in Figure 3.

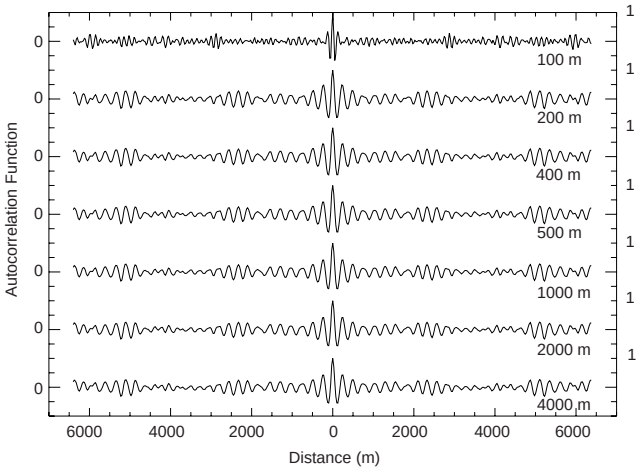

Figure 5. The collapsed autocorrelation function for various high-pass filters.

related to other phase components, then this source of wave groupiness would not be possible.

We tested this assertion using a simulation. We begin with the original image spectrum. We slightly smoothed this spectrum with a Gaussian filter to create an estimate of the ensemble mean image spectrum. For each spectral component in this ensemble mean, we randomly select an amplitude and phase. The phases are uniformly distributed between 0 and 2π and the square of the amplitude has a χ^2-distribution with 2 degrees of freedom. The mean of this χ^2-distribution is equal to the value of the ensemble mean spectrum at each particular spectral component. This allows us to produce any number of Fourier transforms whose mean spectrum is consistent with the ensemble mean spectrum. The phase value for each element of the transform is independent of any other spectral elements.

When we performed these simulations, the resulting autocorrelation functions exhibited none of the groupiness observed in the actual SAR imagery. Thus, we are strongly disposed to associate such groupiness to the nature of ocean surface waves, not processing artifacts.

Discussion of SAR wave-imaging linearity

In a convenient world, the relationship between ocean surface wave slope and SAR image intensity would be linear. However, even for the most linear of SAR geometries (low R/V ratios), the mapping is not perfectly linear. Could the observed crest length statistics and groupiness behavior presented in this paper be a consequence of the lack of perfect linearity?

We conclude not, because such a point-by-point nonlinearity would manifest itself most prominently as a harmonic in the image spectrum. Such harmonics are not present in the images we used. Moreover, if such a nonlinearity were present, we see no way that such a mechanism could introduce large-scale spatial correlations on the order of several kilometers.

Additional nonlinearity is introduced because of the way SARs achieve high azimuth resolution: by relying on the relative motion between the surface and the SAR platform. Could the SAR azimuth image formation process introduce the several kilometer scale variations observed in the autocorrelation function? Could the SAR be remapping radar cross section on spatial scales of several kilometers?

We dismiss this latter possibility by observing that the large-scale spatial correlations are maximized along the wave propagation direction, not the SAR azimuth direction.

Conclusions

The probability of encountering rogue waves depends, in part, on nonlinear wave-wave interactions. These interactions also influence the properties of wave long-crestedness and wave groupiness. We have demonstrated here, that high-resolution SAR imagery indicates that waves are longer-crested and group together in excess of what would be expected if there were no nonlinear interactions. Moreover, the impact of large waves is certainly dependent on the crest length and whether such waves group together. We have provided evidence that the observed behavior is most probably a consequence of the nature of the ocean surface and not of SAR imaging artifacts or the way we processed the data.

Nonetheless, the limited amount of data we have processed thus far is anecdotal in nature. SAR wave imagery over the entire ocean needs to be considered before more statistically significant conclusions can be drawn.

Acknowledgments. We would like to thank the Office of Naval Research for partially sponsoring the research presented here and the National Oceanic and Atmospheric Administration for is continuing support of research in the use of SAR imagery.

References

Alpers, W. R., and C. L. Ruffenach, The effect of orbital motions on synthetica perture radar imagery of ocean waves, *IEEE Trans. Antennas Propag., AP-27*(5), 685–690, 1979.

Beal, R. C., D. G. Tilley, and F. M. Monaldo, Large and small-scale spatial evolution of digitally processed ocean wave spectra from Seasat synthetic aperture radar, *J. Geophys. Res.*, *88*(C3), 1761–1778, 1983.

Bendat, J. S., and A. G. Piersol, *Engineering Applications of Correlation and Spectral Analysis: 2nd Edition*, 472 pp., Wiley-Interscience, 1993.

Donelan, M. A., W. M. Drennan, and A. K. Magnusson, Nonstationary analysis of the directional properties of propagating waves, *J. Phys. Oceanogr., 26*, 1901–1914, 1996.

Forristall, G. Z., Wave crest distributions: observations and second-order theory, *J. Phys. Oceanogr., 30*, 1931–1943, 2000.

Harger, R. O., *Synthetic Radar Systems: Theory and Design*, 36 pp., Academic, 1970.

Kriebel, D. L., and T. H. Dawson, Nonlinear effects of wave groups in nonlinear seas, *J. Offshore Mech. Artic Eng.*, *113*, 142–147, 1991.

Lehner, S., and F. J. Ocampo-Torres, The SAR measurement of ocean waves, in *Second Workshop on Coastal and Marine Applications of SAR*, Longyearbyen, Spitsbergen, Norway, 2003.

Molle-Christensen, E., and A. Ramamonjiarisoaas, Modeling the presence of wave groups in a random field, *J. Geophys. Res.*, *83*, 4117–4122, 1978.

Monaldo, F. M., Measurement of wave coherence properties using spaceborne synthetic aperture radar, *Marine Structures*, *13*, 349–366, 2000.

Phillips, O. M., G. Daifang, and M. A. Donelan, Expected structure of extreme waves in a gaussian sea, Part I: Theory and SWADE buoy measurements, *J. Phys. Oceanogr.*, *23*, 992–1000, 1993.

Swift, C. T., and L. R. Wilson, Synthetic aperture radar imaging of moving ocean waves, *IEEE Trans. Antennas Propag.*, *AP-27*(6), 725–729, 1979.

Wright, J. W., Backscattering from capillary wave with application to sea clutter, *J. Geophys. Res.*, *14*, 749–754, 1960.

Wright, J. W., A new model for sea clutter, *IEEE Trans. Antennas Propag.*, *AP-16*, 217–223, 1968.

F. Monaldo, The Johns Hopkins University Applied Physics Laboratory, 11100 Johns Hopkins Road, Laurel, MD 20723–6099, (e-mail: Frank.Monaldo@jhuapl.edu)

This preprint was prepared with AGU's LaTeX macros v4, with the extension package 'AGU++' by P. W. Daly, version 1.6a from 1999/05/21.